Reference: *Biol. Bull.* **180:** 185–195. (February, 1991)

Calcium-Proton Exchange During Algal Calcification

TED A. McCONNAUGHEY[1]* AND RICHARD H. FALK[2]

[1]*Marine Biological Laboratory, Woods Hole, Massachusetts 02543, and* [2]*Botany Department, University of California, Davis, California 95616*

Abstract. Extracellular calcification by the giant celled alga *Chara corallina* may involve active Ca^{2+} extrusion from the cell in exchange for protons. The following evidence is presented: $CaCO_3$ incrustations accrete largely along the inside, facing the cell, as revealed by X-ray microanalysis using Sr^{2+} and Mn^{2+} as tracers for new mineralization. Inward proton currents are inhibited by the Ca^{2+} transport antagonists Gd^{3+} and La^{3+}. Low Ca^{2+} concentrations inhibit pH banding and photosynthesis, and solutions of low Ca^{2+} activity support more photosynthesis in the presence of additional buffered calcium. The ratio of calcification to photosynthesis in moderately alkaline solutions containing sufficient calcium remains stable at about 1.0 independent of solution Ca^{2+} concentration. Ion specific microelectrodes placed close to the calcified surface sometimes detect increases in Ca^{2+} activity coincident with decreases in proton activity. As the pCa of solution increases, the maximum pH observed at the alkaline surface increases, as does the maximum solution pH which supports electrochemical currents by the cell. Combinations of extracellular pH and pCa approach the calculated thermodynamic limits for ATP driven $2H^+/Ca^{2+}$ exchange against the cytosol.

Introduction

Ca^{2+} ATPase appears to be associated with calcification in various animals and plants (*e.g.*, Klaveness, 1976; Okazaki, 1977; Okazaki *et al.*, 1984; Kingsley and Watabe, 1985). This report explores the possibility that extracellular calcification in characean algae involves active calcium-proton exchange.

Characeans calcify as a by-product of bicarbonate assimilation from alkaline waters (Spear *et al.*, 1969; Raven *et al.*, 1986; Okazaki and Tokita, 1988). The plants extract proton equivalents from the medium along parts of their giant cells, forming alkaline patches or bands that may become heavily calcified. The proton equivalents are extruded elsewhere, forming acidic patches or bands. There, HCO_3^- is apparently protonated to form CO_2, which the plant absorbs (Walker *et al.*, 1980; Smith and Walker, 1980; Price and Badger, 1985). Pericellular carbonic anhydrase and complicated invaginations of the plasma membrane within the acid zones may facilitate CO_2 generation and absorbtion (Price *et al.*, 1985).

Characeans can be more than half $CaCO_3$ by dry weight, and as will be shown here, calcification is often stoichiometric to photosynthesis. Nevertheless, calcification physiology has been largely neglected, and calcification is generally assumed to be independent of active Ca^{2+} transport (*e.g.*, Raven *et al.*, 1986). Various evidence nevertheless suggests that active Ca^{2+} transport might be involved. First, Ca^{2+} ATPases apparently catalyze Ca^{2+} extrusion from cells in exchange for protons (Niggli *et al.*, 1982; Villalobo and Roufogalis, 1986; Rasi-Caldogno *et al.*, 1987; Dixon and Haynes, 1989). Ca^{2+} ATPase could therefore catalyze proton uptake at the site of calcification in *Chara*. Second, characeans are functionally analogous to coccolithophorid algae, which also calcify in an approximate ratio of 1:1 to photosynthesis, but do so intracellularly (*e.g.*, Sikes *et al.*, 1980). Ca^{2+} and carbon presumably traverse the cytoplasm to reach the vesicular site of calcification, and Ca^{2+} ATPase seems to be involved (Klaveness, 1976; Okazaki *et al.*, 1984). Third, molecular CO_2 apparently provides most of the precipitating carbon during calcification by various plants and animals (McConnaughey, 1989a, b, c), including *Chara* (Mc-

---

Received 3 April 1990; accepted 6 November 1990.

*Address communications to: Dr. Ted McConnaughey, U.S. Geological Survey, Box 25046 MS 413, Lakewood, CO 80225.

Abbreviations: CAPS = 3-(cyclohexylamino)propanesulfonate; CHES = 2-(N-cyclohexylamino)ethanesulfonate; MOPS = 2-(N-morpholino)propanesulfonate; PIPES = 1,4-piperazinediethane-sulfonate; TAPS = tris(hydroxymethyl)methylaminopropane sulfonate; TRIS = tris(hydroxymethyl)aminomethane.

Connaughey, in prep). Since HCO_3^- is more abundant in alkaline solutions, its unimportance in calcification suggests that the calcifying region can be fairly isolated from solution. The calcifying cell must therefore supply calcium, and remove the protons generated by the reaction $Ca^{2+} + CO_2 + H_2O = CaCO_3 + 2H^+$. And finally, Ca^{2+} is well known to affect characean photosynthesis and membrane properties associated with pH banding (*e.g.*, Lucas, 1976; Wiesenseel and Ruppert, 1977; Luhring and Tazawa, 1985; Bisson, 1984; Tazawa *et al.*, 1987).

A Ca^{2+} ATPase model and a more conventional proton channel model for characean calcification are illustrated in Figure 1. Both models are elaborated to fit the available data. Ca^{2+} influx into the cell, in the Ca^{2+} ATPase model, occurs within the alkaline band (Fig. 1b) to produce the observed electrogenic character of pH banding (Walker and Smith, 1977). Figure 1c, e shows the use of molecular CO_2 from the plant as the major carbon source for calcification (McConnaughey, in prep.) and the accretion of extracellular calcium deposits from the inside (demonstrated here). Figures 1d and 1f depict non-calcifying conditions, such as when Ca^{2+} or carbon levels are too low to sustain much $CaCO_3$ precipitation. The non-calcifying condition can be experimentally useful, because the H^+ fluxes measured extracellularly then reflect cellular H^+ transport most closely.

The energy (E) required for proton uptake under both models is given by:

$$E = FV(aZ_{Ca} - bZ_H) + RT \ln (Ca_i/Ca_0)^a/(H_i/H_0)^b \quad (1)$$

The terms on the right represent work done against the membrane electrical potential V, and against the membrane chemical gradients. F is the Faraday constant, "a" and "b" are the numbers of Ca^{2+} and H^+ ions transported per cycle, Z is ionic charge, R is the gas constant, and T is Kelvin temperature. Cytoplasmic and external Ca^{2+} and H^+ activities are subscripted "i" and "o," respectively.

For the proton channel model, protons are drawn into the cell by the membrane electrical potential. The thermodynamic limit for passive (E = 0) proton uptake occurs when the membrane electrical and chemical gradient energies balance, yielding a proton Nernst equation:

$$0 = FV + 2.3\ RT(pH_0 - pH_i) \quad (2)$$

For an illuminated cell in alkaline solution, the membrane potential might be around −200 mV and cytoplasmic pH_i might be about 7.5–8.0 (Smith and Raven, 1979; Spanswick and Miller, 1977; Mimura and Kirino, 1984;

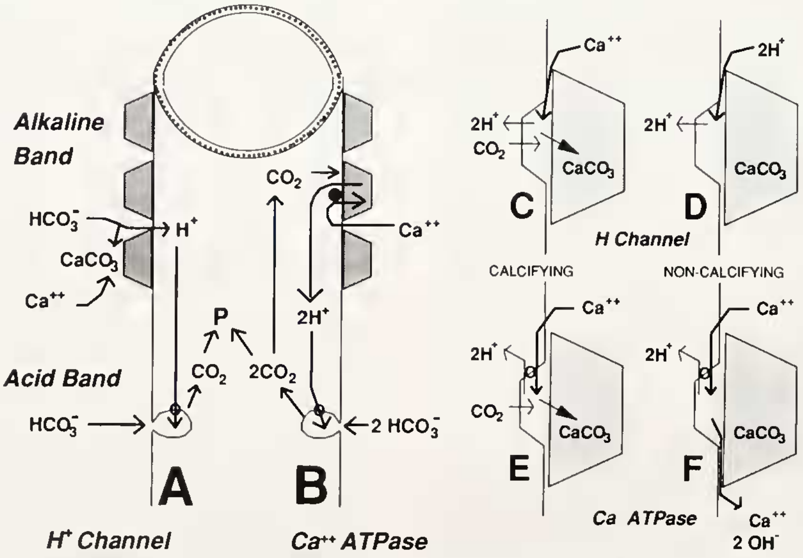

Figure 1. Models of extracellular calcification and its coupling to bicarbonate utilization in *Chara*. Left: schematic of a cell, showing alkaline band at top (with trapezoidal $CaCO_3$ incrustations), and acid band below (with plasmalemmasomes, participating in bicarbonate use). "P" represents photosynthesis. (a) Proton channel model. HCO_3^- diffuses to the alkaline surface and donates a proton, becoming converted to $CO_3^=$, which precipitates with Ca^{2+}. (b) Ca^{2+} ATPase model. ATP driven $2H^+/Ca^{2+}$ exchange alkalinizes the external medium and locally increases its Ca^{2+} concentration. CO_2 diffuses from the cell and reacts with water to yield the protons needed for exchange with Ca^{2+}, and the $CO_3^=$ which precipitates as $CaCO_3$. A 1:1 ration of calcification to photosynthesis is shown for both models. Right: elaborations on the H^+ channel and Ca^{2+} ATPase models for the alkaline band, incorporating inward accretion of $CaCO_3$ incrustations, using CO_2 as the carbon source. Proton channel (c, d) and Ca^{2+} ATPase models (e, f) showing the alkaline band under calcifying (c, e) and non-calcifying conditions (d, f). The ion fluxes detectable externally are highlighted.

Smith, 1984a, b). The maximum pH in the alkaline band would then be about 10.9–11.4, independent of solution Ca^{2+} activity.

For ATP-driven $2H^+/Ca^{2+}$ exchange, the energy of ATP hydrolysis (E) is about −50 to −55 KJ/mol (*e.g.*, Kishimoto *et al.*, 1984). The electrical term in eq. (1) drops out, leaving

$$E/2.3RT = (pCa_0 - pCa_i) - 2(pH_0 - pH_i) \qquad (3)$$

Cytoplasmic $pCa_i = -\log\{Ca^{2+}{}_i\}$ is about 6.9 (Miller and Sanders, 1987). Equation 3 describes a line in (pH_0, pCa_0) space having a slope of 1/2, and displaced from the composition of the cytosol, (pH_i, pCa_i), by 4.4 to 4.8 pH units.

The present experiments look for evidence that $CaCO_3$ incrustations accrete from the inside, as would be expected if the plant supplies the precipitating calcium and carbon. Proton and calcium specific microelectrodes search for regions of elevated Ca^{2+} and depressed H^+ activities along the calcifying surface. The combinations of calcium and proton activities are compared with the thermodynamic constraints of ATP driven $2H^+/Ca^{2+}$ exchange against the cytosol. Calcium transport antagonists are used to inhibit proton uptake. And the stoichiometry of calcification to photosynthesis is examined to see if calcium merely diffuses to the calcification site. In the end, the Ca^{2+} ATPase model offers some advantages, but presents some interesting difficulties. The discussion touches on how the plant uses calcification as a photosynthetic adaptation.

Materials and Methods

The present experiments used male plants of *Chara corallina* from South Australia, provided by Bill Lucas. Plants were maintained in the laboratory, in aquaria initially containing "CPW/B" solution (in m*M*, $CaCl_2$ 0.2, $NaHCO_3$ 1, NaCl 1, KCl 0.2) overlying 5–20 cm mud. Nutrients and additional calcium and carbon were sometimes added to stimulate growth and calcification. Cool white fluorescent lights provided illumination.

Regions of new mineralization were identified by X-ray microanalysis. Plants first accumulated $CaCO_3$ in a medium containing (in m*M*) $CaCl_2$ 2, $NaHCO_3$ 2, $CaSO_4$ 0.2, KCl 0.2, and NaCl 1, and were then transferred to media containing additional $SrCl_2$ 1, and $MnSO_4$ 0.1, to label regions of new mineralization. Cells showing heavy calcification and good cytoplasmic streaming were rapidly frozen in liquid nitrogen slush, fractured, and given a thin coating of aluminum by vacuum evaporation (Emscope SP2000) at −196°C, to increase surface conductivity. Frozen hydrated specimens were transferred under vacuum to the cryostage of a scanning electron microscope (Hitachi S800) equipped with a solid state X-ray spectrometer (Kevex 8000 series). Secondary electron mode images provided details of surface morphology. X-ray maps, line scans, and area scans made with an accelerating voltage of 15 KeV revealed distributions of Ca, Sr, and Mn.

Rates of calcification and photosynthesis were estimated from changes in the alkalinity and total dissolved inorganic carbon content of solution. Alkalinity was measured by acidometric titration using the Gran method (Stumm and Morgan, 1970). Heavily calcified plants were incubated in stoppered flasks at 25°C under a mixture of fluorescent and incandescent lights for 6–8 h. Solutions initially contained (in m*M*/l) $NaHCO_3$ 1, NaCl 1, KCl .2, and 0–50 m*M* $CaCl_2$, pH 8 to 8.2, adjusted with NaOH. Calcification was calculated as half the change in alkalinity, and photosynthesis was calculated as the change in total carbon minus calcification.

In experiments designed to see whether buffered Ca^{2+} stimulated photosynthesis in solutions of low Ca^{2+} activity, photosynthesis was monitored using an oxygen electrode (Orion 97–08). Wide mouth jars (500 ml) containing about 5 g of algae were filled with solutions prepared from partially degassed, deionized water, and capped underwater to exclude air bubbles. Control solutions contained (in m*M*) $CaCl_2$ 0.05, KCl 0.1, NaCl 1, $NaHCO_3$ 1.8, and Na_2CO_3 0.2. Test solutions contained an additional 0.8 m*M* $CaCl_2$ and sodium citrate (1.5 m*M*). These solutions exhibited the same Ca^{2+} activity, using a Ca^{2+} specific microelectrode. A relatively high pH (9.1) ensured that the plants obtained most of their carbon through the physiology associated with pH banding. Half of the plants had been mostly decalcified before the experiment by soaking them for 2 days in a solution containing 10 m*M* MES buffer, initial pH 5.2. Cool white fluorescent lights provided illumination during 2–3 h incubations at about 25°C.

The effect of calcium transport antagonists on inward proton currents were investigated by exposing an illuminated cell to $LaCl_3$ or $GdCl_3$, while measuring proton uptake with an extracellular vibrating H^+ specific microelectrode (Kühtrieber and Jaffe, 1990). The cell was mounted in an open Petri dish (solution volume about 3 ml) and perfused at a rate of 0.08 ml/s with a solution containing, in m*M*: $CaCl_2$ 0.2, KCl 0.2, NaCl 1.0, TRIS 5, pH adjusted to 8.3 with NaOH. Fiberoptic lights provided illumination. The proton electrode vibrated perpendicularly to the cell over an excursion of 10 μ, at a frequency of 0.5 Hz, at a distance of about 10 μm from the cell. 4 μMoles of the lanthanide was added to the input stream without changing flow rate. The signal here is the voltage difference registered by the electrode as it moves back and forth near the cell. A proton gradient of one pH unit within the sampled region ideally yields a signal of about 58 mV, although in practice the signal is smaller. Fluxes of proton equivalents carried by H^+, OH^-, and protonated TRIS buffer were calculated from Fick's first law, using diffusion coefficients 93, 53, and 7×10^{-6} cm^2/s, respectively, and concentrations calculated from the measured pH. In the case illustrated, the pH at the electrode was about 9 before adding the lanthanides. The voltage field arising from net charge uptake by the alkaline band introduces only a small bias to the pH signal; relative to background solution, the alkaline band might show a voltage differential of about −4 mV, while the pH gradient of around 2 units produces a voltage signal of about −120 mV.

Ca^{2+} and H^+ activities at the alkaline surface of the cell were measured using stationary ion specific microelectrodes, constructed as described by Borelli *et al.* (1985). Electrodes were connected to a high impedance amplifier (World Precision Instruments FD223), with output to a chart recorder. Additional potential sensing electrodes were sometimes used as well. The pericellular electrical field (about −4 mV relative to background) biased pH and pCa measurements by about +.07 and 0.14 pCa unit, respectively. The cells were exposed to buffered solutions of various calcium concentrations, usually lacking dissolved inorganic carbon to discourage calcification. Fiber optic lights provided illumination.

In experiments comparing pericellular pH against a thermodynamic model for $2H^+/Ca^{2+}$ exchange, the pH data represent the highest values observed during electrode scans of the cell surface, and during observations of several minutes duration at particularly alkaline locations. Solution pCa was calculated from solution Ca^{2+} concentrations and ionic strength, using Davies' individual ion activity coefficient (see Stumm and Morgan, 1970), or measured using an Orion 93–20 electrode for solutions containing citrate. In experiments comparing simultaneous variations in pericellular pH and pCa, H^+ and Ca^{2+} electrodes were placed close together near the alkaline surface of the cell, and the intensity of pH banding either fluctuated spontaneously or was modulated by turning the light off and on. In the examples shown, the medium contained MOPS (5 m*M*) and citrate (2 m*M*), plus NaOH and $CaCl_2$ to produce pH 7.98, pCa 3.89.

Extracellular electrical currents were measured using a vibrating probe electrometer (Jaffe and Nuccitelli, 1974). The probe vibrated perpendicular to the cell surface, approximately 30–50 μm from the cell while the cell moved by on a motorized stage. Fiberoptic lights provided illumination. Most experiments used nominally carbon-free solutions containing (in m*M*) KCl 0.2, NaCl 1, and a zwitterionic buffer (MOPS, PIPES, EPPS, CHES, or CAPS, 5 m*M*), pH adjusted to the desired value using NaOH. At the chosen concentration of $CaCl_2$ (0.1–50 m*M*), the cell was repeatedly scanned along its length for electrical activity while solutions of progressively higher pH or Ca^{2+} concentration were added. The cell was allowed to adjust in each solution for at least 30 min. Electrical currents were calculated from the electrical conductivity of solution, using Ohm's law. The example shown used a divided chamber, so that opposite halves of the cell were exposed to different solutions. Cytoplasmic streaming between the two halves was uninterrupted. The "control" half was bathed in CPW/B, while the "test" half went from CPW/B to carbon-free solutions containing zwitterionic buffers and 20 m*M* $CaCl_2$ at progressively higher pH.

Results

Mineralization patterns

Calcified cells exposed to solutions enriched in Sr and Mn accumulate significant Sr and Mn mainly along the inward surface of $CaCO_3$ incrustations (Figs. 2, 3, 4). This distribution suggests metal transport from the cell to the extracellular site of deposition, although diffusion along the cell wall is also possible. Mn/Sr ratios are spatially variable, suggesting some elemental segregation during transport or precipitation. This is indicated by variations in the relative intensities of their X-ray peaks observed in area scans. Some of this variability is visible in the X-ray maps presented in Figure 3.

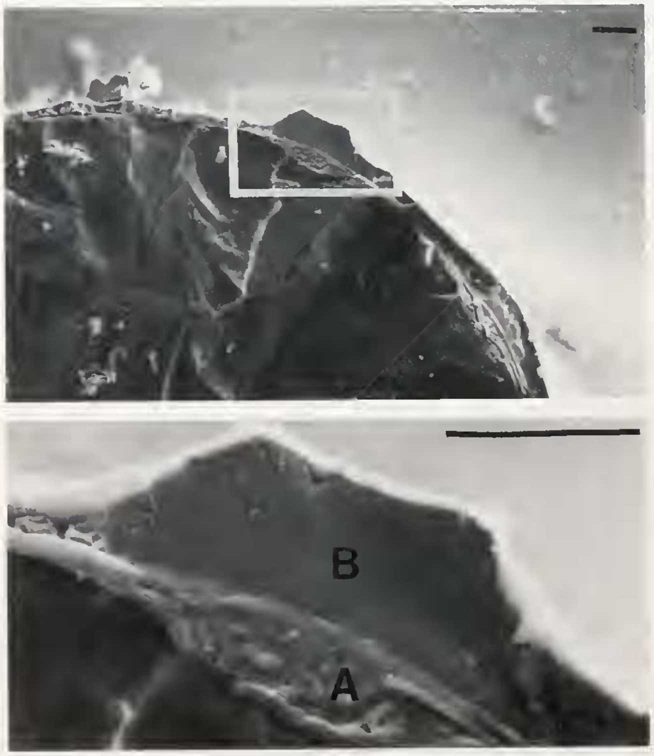

Figure 2. Scanning electron micrograph of frozen, hydrated cell labeled with Sr^{2+} and Mn^{2+}, showing extracellular $CaCO_3$ incrustations, with inward dimpling of the cell and apparent duplication of the cell wall. Magnification: top 162×, bottom 830×. Scale bar = 30 μ.

Figure 3. Distributions of Ca (yellow), Sr (blue), and Mn (red) in an extracellular $CaCO_3$ deposit, visualized by X-ray mapping of a frozen, hydrated cell exposed to Sr^{2+} and Mn^{2+} after first accumulating significant $CaCO_3$.

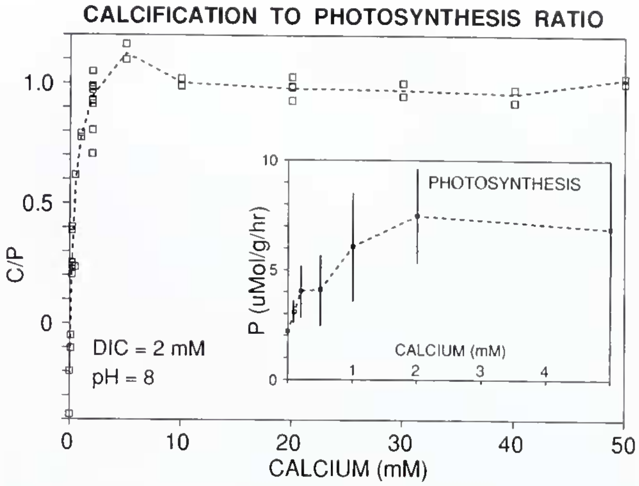

Figure 5. Ratio of calcification to photosynthesis near pH 8 as a function of Ca^{2+} concentration. Inset: inhibition of photosynthesis by low Ca^{2+} concentrations. Error bars: 1 S.D.

Sr and Mn accumulations presumably consist of divalent metal carbonates and MnO_2, the latter inferred from its dark color. Manganese oxidation, $Mn^{2+} + H_2O + ½O_2 = MnO_2 + 2H^+$, is favored in the alkaline, oxygen-rich environment of the plant surface. More or less pure Mn accumulations, based on relative X-ray counts for Mn, Sr, and Ca, sometimes occur beneath $CaCO_3$ incrustations, even when the incubating medium contains considerably more Ca^{2+} and Sr^{2+}. Mn enrichment may reflect kinetics of transport or precipitation, and was probably assisted by oxidation of Mn^{2+} to Mn^{4+}, thus producing a less soluble, non-transportable cation.

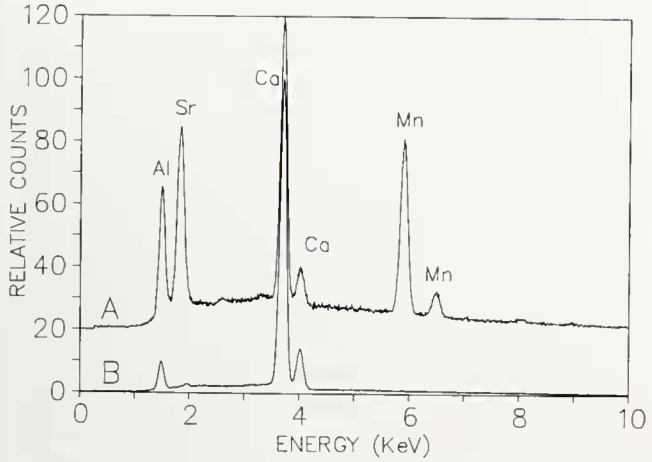

Figure 4. X-ray spectra taken at points "A" and "B" of cell shown in Figure 2. Spectra correspond to materials deposited after (A) and before (B) addition of Sr^{2+} and Mn^{2+} to the medium. X-ray counts are scaled relative to the Ca peak (100%); spectrum A has been shifted upwards by 20% for clarity.

Indentations of the cell and apparent duplications of the cell wall sometimes occur underneath $CaCO_3$ incrustations (Fig. 2). Non-calcified regions of the cell lack such features. Calcification within the cell wall may force the plasma membrane inward, followed by the secretion of a new wall. This scenario again suggests $CaCO_3$ accretion to the inward side of $CaCO_3$ incrustations, and $CaCO_3$ adhesion to the cell wall.

Physiological stoichiometry

The molar ratio of calcification to photosynthesis (C/P), determined using the pH-alkalinity method, is relatively constant at about 1.0 for Ca^{2+} concentrations between 2 and 50 m*M* (pH 8, 1 m*M* $NaHCO_3$) (Fig. 5). Controls (dark, no algae, or boiled algae) show little calcification, even at 50 m*M* $CaCl_2$.

The Ca^{2+} ATPase model (Fig. 1) correctly predicts the 1:1 C/P ratio, provided the calcifying region is fairly isolated from bulk solution. Each CO_2 precipitated at the alkaline band yields $2H^+$, which the plant uses to generate $2CO_2$ at the acid band. Calcification uses one CO_2, leaving one for photosynthesis, yielding a 1:1 C/P ratio. The proton channel model would predict lower C/P ratios, increasing with Ca^{2+} concentration, because a diffusion pathway must exist to the calcifying region. OH^- and $CO_3^=$ can therefore diffuse away. These results consequently favor the Ca^{2+} ATPase model.

Proton cycling involves calcium

Low Ca^{2+} concentrations inhibit photosynthesis (Fig. 5, inset). This inhibition appears to involve Ca^{2+} fluxes, because plants incubated at the same low Ca^{2+} activity show more photosynthesis if additional buffered Ca^{2+} is added to solution (Table I). The rate of photosynthesis and the stimulation by buffered Ca^{2+} are greater with calcified than with decalcified plants (two way ANOVA, both factors and interactions significant at $P < 0.05$).

Proton uptake at the alkaline band, measured using a vibrating H^+ specific electrode, is inhibited by the Ca^{2+} transport antagonists Gd^{3+} and La^{3+} (Fig. 6). In this example, the electrode was positioned over a point showing particularly strong alkalinization. Gd^{3+} reduced the signal registered by the vibrating electrode by about half, but the cell soon recovered about 80–90% of its former signal. Subsequent treatment with La^{3+} reduced the signal more strongly, and H^+ uptake did not recover for over an hour. Before adding the lanthanides, the voltage difference signal registered by the vibrating electrode (about 7 mV at pH 9) corresponds ideally to a flux of proton equivalents around 2 nMoles cm^{-2}/s, carried mostly by OH^- and TRIS buffer (calculation, Fig. 6 inset).

The alkaline bands of *Chara* can turn on and off independently, sometimes without obvious provocation, so reductions in the pH gradient are not necessarily proportional to pathology. The pH gradient is also affected by $CaCO_3$ dissolution at the plant surface, and by ion pairing and precipitation of the introduced lanthanides. The effects here appear to be mostly physiological, however. Perfusion of the chamber should have brought solution pH back to normal within a few minutes (theoretical dilution time about 38 s).

An approximately 2–3 min oscillation in apparent H^+ influx is observed in this experiment (Fig. 6). Such oscillations are detected using various techniques (Fisahn *et al.*, 1989), and can sometimes be induced by adding Ca^{2+} to the medium.

Electrochemical detection of calcium efflux

Both the Ca^{2+} ATPase and proton channel models predict Ca^{2+} diffusion toward the alkaline surface under calcifying conditions. The Ca^{2+} ATPase model also predicts localized Ca^{2+} efflux, which, in principle, should be detectable with Ca^{2+} specific microelectrodes. This efflux might be difficult to detect, however. It may occur underneath $CaCO_3$ crystals or within an endomembrane system, and calcification may consume it before it is detected externally. More importantly, Ca^{2+} influx and efflux must both occur within the alkaline band to produce its electrogenic character (Fig. 1b), regionally cancelling the Ca^{2+} efflux signal. Therefore, detection requires a local asymmetry between Ca^{2+} influx and efflux under non-calcifying conditions (Fig. 1f).

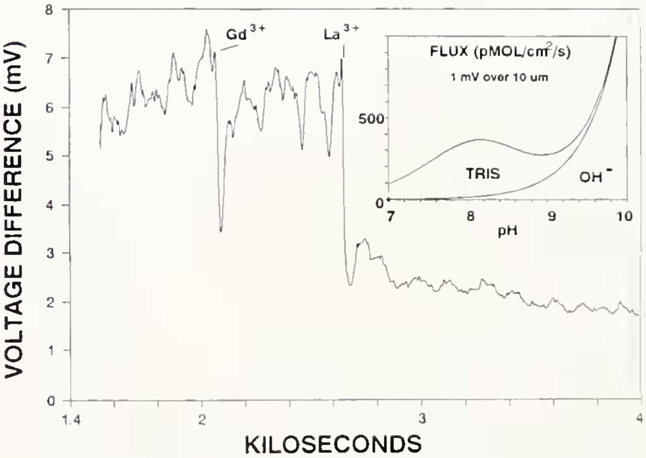

Figure 6. Inhibition of proton influx by La^{3+} and Gd^{3+}, measured with a vibrating proton specific electrode. Ordinate: voltage difference registered by the electrode between the extremes of its 10 micron excursion perpendicular to the cell. Inset: apparent proton influx calculated from a diffusion model, as a function of pH at the probe, for a signal of 1 mV over an excursion of 10 microns. Fluxes scale almost linearly with excursion and voltage.

Table I

Stimulation of photosynthesis by buffered calcium, at low solution calcium activity. Photosynthesis estimated by oxygen evolution, in micromoles O_2 per gram wet weight per hour, with standard deviation ($n = 10$)

	Solution		
	Unbuffered	Buffered	Change
Calcified	6.43 ± 0.67	8.11 ± 0.68	+26%
Decalcified	4.48 ± 0.10	5.29 ± 0.41	+18%

Such conditions encourage $CaCO_3$ dissolution and Ca^{2+} leaching from the cell wall. The resulting increase in pericellular Ca^{2+} concentration may be confused with the effects of $2H^+/Ca^{2+}$ exchange. The former effect will be most pronounced at low pH, while the latter will be associated with high pH. Simultaneous pH observations are therefore needed to distinguish these two cases.

Increases in Ca^{2+} activity (pCa decreases) are often observed coincident with pH decreases (Fig. 7a), suggesting Ca^{2+} leaching or $CaCO_3$ dissolution. Small drops in pCa are also observed coincident with pH increases (Fig. 7b), suggesting $2H^+/Ca^{2+}$ exchange. At one point in the case illustrated, the apparent pericellular Ca^{2+} activity increases about 30% as the pH rises from 8.2 to 9.8. The actual Ca^{2+} activity presumably increased even more, because the alkaline band develops a pericellular electrical field of around −4 mV when it turns on. This biases the Ca^{2+} electrode toward higher apparent pCa by about $-4/-28 = 0.14$ pCa unit. The increase in pericellular Ca^{2+} due to

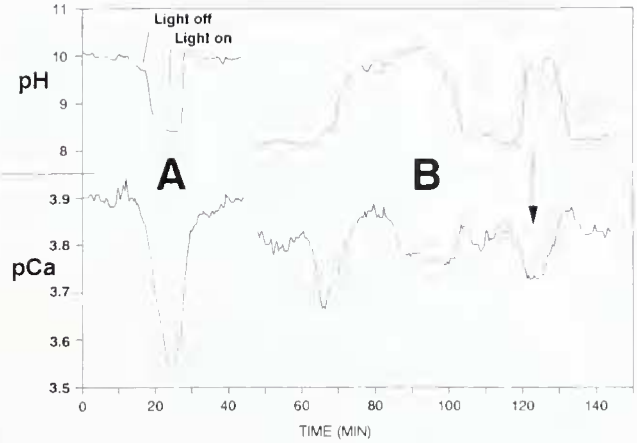

Figure 7. Extracellular pH and pCa measured with stationary ion specific electrodes placed close to the calcified surface of a cell under non-calcifying conditions. (A) Positive correlation between pH and pCa, probably caused by increased $CaCO_3$ dissolution or leaching at low pH. (B) Anticorrelation between pH and pCa, suggesting calcium-proton exchange.

$2H^+/Ca^{2+}$ exchange must also be sufficient to overcome the decrease in pericellular Ca^{2+} at high pH, caused by reductions in $CaCO_3$ dissolution and Ca^{2+} leaching from the cell wall.

Thermodynamics

The maximum pH observed at the alkaline surface using microelectrodes approaches the thermodynamic limit for ATP driven $2H^+/Ca^{2+}$ exchange, calculated using eq. 3 (Fig. 8). The approach is closest at high solution Ca^{2+} activities (low pCa). As pCa^{2+} increases, the maximum pH also increases, although not as much as allowed by thermodynamics. At pCa >4, higher pH readings are obtained in the presence of the weak Ca^{2+} buffer citrate, suggesting that the rate of Ca^{2+} supply to the cell may limit proton uptake. All pericellular pH, pCa observations fall within the thermodynamic constraints for ATP driven $2H^+/Ca^{2+}$ exchange, and the Ca^{2+} dependence for pericellular pH provides some support for the Ca^{2+} ATPase model.

The pH and pCa in large culture vessels containing *Chara* also approach the calculated thermodynamic limits for $2H^+/Ca^{2+}$ exchange (Fig. 8). The most extreme conditions observed (pH 10.78, pCa 4.30) are close to the most extreme conditions observed at the cell surface with microelectrodes. Rather high pericellular pH (about 10.7) is observed transiently in Ca^{2+} free solutions, but pH banding eventually collapses, consistent with a Ca^{2+} requirement for banding. Internal Ca^{2+} stores, perhaps supplemented by $CaCO_3$ dissolution and Ca^{2+} leaching from the cell wall, may support banding for awhile.

Extracellular electrical currents

The ion fluxes associated with pH banding create extracellular current loops which can be measured with a vibrating probe electrometer. These currents persist until solution pH is raised above a critical value, at which point the currents cease or may reverse with much diminished amplitude. The solution pH at which current cessation occurs varies with solution Ca^{2+} activity in more or less the same way as the extracellular pH data in Figure 8. The Ca^{2+} dependence suggests that proton uptake is coupled to Ca^{2+} expulsion.

Presumably, as $2H^+/Ca^{2+}$ exchange becomes impossible, cytosolic Ca^{2+} rises and inhibits Ca^{2+} influx (see Eckert and Chad, 1984). The proton ATPase of the acid band shuts down as the cytoplasm becomes alkalinized (due to cessation of proton uptake) and the membrane potential increases (due to cessation of Ca^{2+} uptake). Consequently, even though $2H^+/Ca^{2+}$ exchange is electrically silent, preventing this exchange can stop extracellular electrical activity.

Figure 9 illustrates an experiment in which a cell is placed in a divided chamber, and increasingly alkaline solutions containing 20 mM $CaCl_2$ (pCa = 2.1) are applied to the right (test) side. The left (control) side remains at pH 8.2, pCa = 3.8. Cytoplasmic streaming between the two sides is uninterrupted. As the test side approaches the calculated thermodynamic limits for ATP driven $2H^+/Ca^{2+}$ exchange, its currents diminish, but currents on the control side are unaffected. In the last test solution (pH 10.0, pCa 2.1), banding is strongly suppressed and an ap-

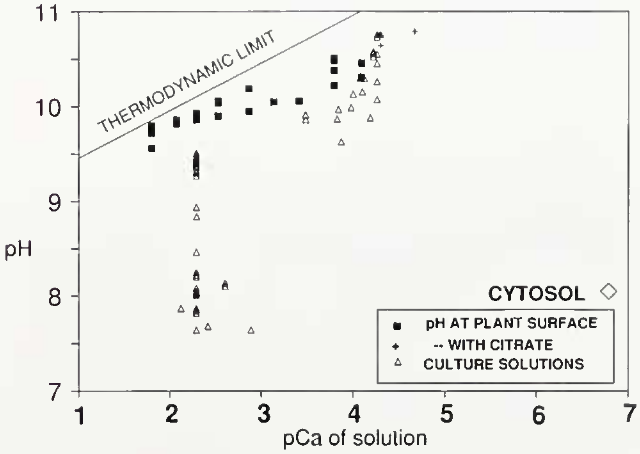

Figure 8. pH observations at the alkaline surface as a function of solution Ca^{2+} activity. Diagonal line: calculated thermodynamic limits for ATP driven $2H^+/Ca^{2+}$ exchange between the cytosol and external solution, assuming E(ATP) = 50 KJ/mol. Symbols: (Diamond) assumed cytosolic composition, pH = 8, pCa = 6.9. (Squares) maximum pH observed at alkaline surface under experimental conditions, without citrate. (+) Same, with citrate. (△) Combinations of solution pH and pCa observed in large vat cultures.

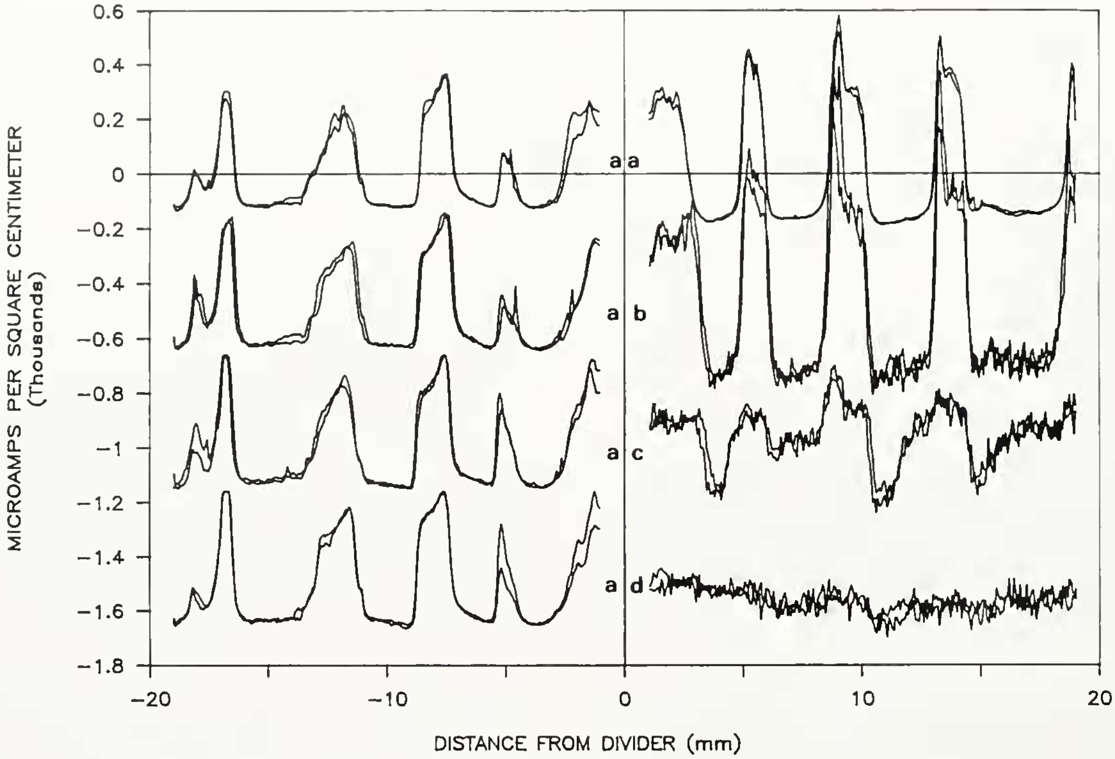

Figure 9. Extracellular currents measured using a vibrating voltage probe. Cell was placed in a divided chamber, and solution on the right side was replaced with solutions having higher Ca^{2+} activity and progressively higher pH. Duplicate scans are shown in each medium, and cell responses to different media are offset by −500 $\mu A/cm^2$. Positive currents denote regions of positive current influx to cell (alkaline bands). Solutions contained (in m*M*) NaCl 1, KCl 0.2, plus the following additions: (a) $CaSO_4$ 0.2, $NaHCO_3$ 1, pH 8.2. (b) $CaCl_2$ 20, CHES 5, pH 9.0. (c) $CaCl_2$ 20, CAPS 5, pH 9.8. (d) $CaCl_2$ 20, CAPS 5, pH 10.0).

parent efflux of positive charge prevails over the test side of the cell. The control side does not appear to compensate, so if real, this current efflux should hyperpolarize the cell.

Discussion

Antecedents to the Ca^{2+} ATPase model for *Chara* extend back at least to 1829, when Bishoff (cited in Pringsheim, 1888) suggested that characean lime deposits grow from the inside. Classical works on bicarbonate use also favored calcium and carbon movement through the polarized leaves of calcareous aquatic angiosperms and characeans to reach the site of mineralization (Arens, 1933, 1938, 1939). Kishimoto *et al.* (1984) suggested that proton uptake in *Chara* might occur through an electroneutral proton cotransport or countertransport system. Many aspects of the Ca^{2+} ATPase model have therefore been discussed.

The Ca^{2+} ATPase model correctly predicts the data presented here. Sr^{2+} and Mn^{2+} accumulate largely along the inner surface of $CaCO_3$ incrustations, facing the cell. Increasing the Ca^{2+} concentration in solution (from 2 to 50 m*M*) has a minimal effect on the ratio of calcification to photosynthesis, suggesting that diffusion to the calcification site can be minimal. Ca^{2+} transport antagonists interfere with H^+ uptake. In solutions of low Ca^{2+} activity, additional "buffered" Ca^{2+} enhances photosynthesis and proton uptake. Pericellular Ca^{2+} activities sometimes increase simultaneously with stronger alkalization. Combinations of extracellular Ca^{2+} and H^+ activities are thermodynamically compatible with ATP driven $2H^+/Ca^{2+}$ exchange, and the maximum pH at the alkaline band increases with pCa, as would be expected if Ca^{2+} extrusion accompanies proton uptake.

Most of the precipitating carbon also appears to be supplied by the cell as CO_2 (McConnaughey, in prep.). This further implies that the calcifying region can become isolated from bulk solution. Consequently, the cell must supply Ca^{2+}, and remove protons in 1:2 stoichiometry, as indicated by the reaction $Ca^{2+} + CO_2 + H_2O = CaCO_3 + 2H^+$.

The data are less supportive of the proton channel model, which offers no explanation for the Ca^{2+} dependence of photosynthesis, or the elevations of pericellular Ca^{2+} coincident with H^+ depletion. The diffusion pathway to the site of calcification creates additional conceptual problems. Why won't it accept OH^- and $CO_3^=$, which should diffuse away from the cell, reducing the ratio of calcification to photosynthesis to values below 1.0, and making it dependent on the Ca^{2+} concentration, or phosphate, which fails to precipitate where Sr and Mn do (McConnaughey, in prep.)?

Most of the published data appears compatible with the Ca^{2+} ATPase model. Both models attribute the extracellular current influx in the alkaline band largely to Ca^{2+} under calcifying conditions, and to H^+ equivalents under non-calcifying conditions (Fig. 1). Membrane hyperpolarizations are caused by electrogenic H^+ extrusion in the acid band under either model. Increased membrane conductivity at high pH (Bisson and Walker, 1980, 1982) might result from more favorable thermodynamics for the proton ATPase of the acid band, reversibility of $2H^+/Ca^{2+}$ exchange, and perhaps opening of additional ion channels (*e.g.*, Kikuyama *et al.*, 1984).

Calcium transport

Certain caveats apply to the thermodynamic analysis of Ca^{2+} transport attempted here. Pericellular pCa varies locally, and depressions relative to solution values are likely at high pCa (Fig. 7). Cytoplasmic pH and pCa may also vary. Extracellular and intracellular activity scales may be offset with respect to each other. The slope of the extracellular pH data is closer to 1/3 than 1/2, but pH is too high for ATP driven $3H^+/Ca^{2+}$ exchange. $4H^+/2Ca^{2+}$ exchange is likewise excluded. Several factors may contribute to the fall-off from the limits calculated for $2H^+/Ca^{2+}$ exchange at high pCa. As noted above, Ca^{2+} extrusion may locally depress pCa below ambient values. Ca^{2+} diffusion toward the cell may limit the rate of Ca^{2+} and H^+ cycling, as suggested by the higher pH values and photosynthetic rates obtained with buffered Ca^{2+}. Finally, the diffusion of alkalinity from the plant surface increases enormously as pericellular pH increases (see Fig. 6 inset), so if the proton flux remains constant, diffusion should reduce pericellular pH most strongly at high pCa. In summary, there are many reasons why the data might fall short of the thermodynamic limit, even if the plant operates close to the limit. The more interesting feature is that the plant apparently approaches the thermodynamic limit.

Why are extracellular H^+ fluxes so much easier to detect than Ca^{2+} fluxes? The difference, presumably, is that Ca^{2+} influx and efflux occur close together, while proton fluxes must be separated to create the acid bands needed for bicarbonate assimilation. Proton electrodes are also twice as sensitive as Ca^{2+} electrodes, and proton fluxes should be twice as large.

The Ca^{2+} ATPase model postulates high rates of Ca^{2+} cycling through the cell, around 100 pMol $cm^{-2}\ s^{-1}$ within the alkaline band of *Chara*. $^{45}Ca^{2+}$ exchange rates are generally less than 3 pMol $cm^{-2}\ s^{-1}$, measured over the whole cell (Spanswick and Williams, 1965, Hayama *et al.*, 1979; MacRobbie and Banfield, 1988). Some experiments employed conditions unfavorable to pH banding, but the disparity between inferred and published steady state $^{45}Ca^{2+}$ fluxes nevertheless requires further study. Low Ca^{2+} exchange rates may be caused by containment of fluxes to the cortical cytoplasm of the alkaline band, with little exchange into major cellular Ca^{2+} reservoirs such as the vacuole, chloroplasts, or mitochondria. The available evidence supports this possibility. Extracellular electrical currents presumably reflect Ca^{2+} uptake mainly within the alkaline bands. When cells are placed in a divided chamber with Mn^{2+} on one side, Mn precipitation is visible only on that side, suggesting minimal transport along the cell. $^{45}Ca^{2+}$ fluxes measured during repeated electrical stimulation yield values around 60 pMol $cm^{-2}\ s^{-1}$, measured over the whole cell, at 1 m*M* external Ca^{2+} (Hayama *et al.*, 1979). The metabolic machinery needed for large fluxes therefore appears to be present.

An analogy to coccolithophorid algae is instructive. Calcification in these algae occurs within intracellular vesicles, so both calcium and carbon presumably traverse the cytoplasm to reach the calcification site. Ca^{2+} ATPase apparently participates in calcification (Klaveness, 1976; Okazaki *et al.*, 1984). Sufficient data are sometimes available to estimate Ca^{2+} fluxes. For example, *Emiliania huxleyi* calcifies at a rate of around $5–7 \times 10^{-18}$ moles/s, and the surface area of the finished coccolith is around $1–1.5 \times 10^{-7}\ cm^2$ (Paasche, 1964; Klaveness, 1976; Sikes *et al.*, 1980). Therefore, the trans-membrane Ca^{2+} flux may be 30–50 pMol $cm^{-2}\ s^{-1}$. This is of the same magnitude as estimated for *Chara*.

Because cytosolic "free" Ca^{2+} concentrations are uniformly rather low, large trans-cellular Ca^{2+} fluxes presumably involve Ca^{2+} rich vesicles, vacuoles, reticula, etc. Total Ca^{2+} concentrations in characean cytoplasm and vacuoles is in the millimolar range (Okihara and Kiyosawa, 1988). To the extent that cytosolic free ion concentrations pose a transport problem, the issue may be more acute with protons. The proton fluxes are presumably twice as large and involve longer distances.

Applicability to other organisms

If Ca^{2+} ATPase underlies extracellular calcification in *Chara* and intracellular calcification in coccolithophorids, it might contribute similarly elsewhere. For example, large Ca^{2+} dependent proton influxes, sensitive to lanthanides, also occur at the calcified rhizoid of the siphonaceous marine alga *Acetabularia* (McConnaughey, in prep.).

Coupling calcification to photosynthesis

Although a photosynthetic organism may loose CO_2 to calcification, it gains two protons for each carbon lost. In mildly alkaline waters, these $2H^+$ potentially enable it to convert $2HCO_3^-$ to $2CO_2$, yielding a net gain of one CO_2 for photosynthesis. An approximately 1:1 ratio of calcification to photosynthesis is observed not only in *Chara*, but sometimes also in coccolithophorid algae (Paasche, 1964; Sikes *et al.*, 1980), calcareous seaweeds (Pentecost, 1978), and invertebrate-algae symbioses (Goreau, 1963; Barnes and Taylor, 1973; Duguay and Taylor, 1978; Kuile *et al.*, 1989). In the symbioses, the animal calcifies while the algae use the CO_2. Rapid and massive calcification may exceed structural or defensive uses for $CaCO_3$, and coccolithophorids, for example, discard excess scales to remain suspended in the water. Corals build up huge skeletal mounds but occupy only the top few millimeters. No structural or defensive use of $CaCO_3$ is obvious in *Chara*.

Proton cycling theoretically allows organisms to generate pericellular CO_2 concentrations well above ambient (Walker *et al.*, 1980). Photosynthesis generally saturates at CO_2 concentrations higher than the atmospheric equilibrium value (*e.g.*, Smith and Walker, 1980), and far higher than present in many natural waters subjected to strong photosynthesis. Elevating CO_2 concentrations (by protonating HCO_3^-) therefore increases carboxylation rate. Many aquatic plants and invertebrate-algae apparently promote photosynthesis through proton cycling. In this context, protons, rather than $CaCO_3$, may be the principle product of calcification.

From a geochemical perspective, biologically precipitated carbonates comprise one of the more abundant crustal materials, and represent the principle biogeochemical reservoir for carbon (Garrels *et al.*, 1976). Because organisms often calcify much faster than the ambient media in which they live, biological calcification may provide an important brake on the photosynthetic alkalinization of natural waters, and thereby affect such processes as the partitioning of CO_2 between the oceans and the atmosphere.

Acknowledgments

Primary funding was provided through NSF fellowship DCB-8807613 to Ted McConnaughey. W. J. Lucas and L. F. Jaffe contributed laboratory facilities. The authors are grateful to J. Fisahn, W. Kühtreiber, A. Miller, and A. Shipley, for their assistance, and to D. McCorkle, A. Kuzerian, C. Barr, and others for their enthusiasm and helpful comments.

Literature Cited

Arens, K. 1933. Physiologisch polarisierter Massenaustausch und Photosynthese bei submersen Wasserpflanzen. I. *Planta* **20:** 621–658.

Arens, K. 1938. Manganablagerungen bei Wasserpflanzen als Folge des Physiologisch polarisierten Massenaustausches. *Protoplasma* **30:** 104–129.

Arens, K. 1939. Physiologische Multipolaritat der zelle von *Nitella* wahrend der Photosynthese. *Protoplasma* **33:** 295–300.

Barnes, D. J., and D. L. Taylor. 1973. *In situ* studies of calcification and photosynthetic carbon fixation in the coral *Montastrea annularis*. *Helgol. Wiss. Meeresunters* **24:** 284–291.

Bisson, M. A. 1984. Calcium effects on electrogenic pump and passive permeability of the plasma membrane of Chara corallina. *J. Membrane Biol.* **81:** 59–67.

Bisson, M. A., and N. A. Walker. 1980. The *Chara* plasmalemma at high pH. Electrical measurements show rapid specific passive uniport of H^+ or OH^-. *J. Membrane Biol.* **56:** 1–7.

Bisson, M. A., and N. A. Walker. 1982. Control of passive permeability in the *Chara* plasmalemma. *J. Exp. Bot.* **33:** 520–532.

Borelli, M. M., W. G. Carlini, W. C. Dewey, and R. R. Ransom. 1985. A simple method for making ion-selective microelectrodes suitable for intracellular recording in vertebrate cells. *J. Neurosci. Methods* **15:** 141–154.

Dixon, D. A., and D. H. Haynes. 1989. Ca^{2+} pumping ATPase of cardiac sarcolemma is insensitive to membrane potential produced by K^+ and Cl^- gradients but requires a source of counter-transportable H^+. *J. Membr. Biol.* **112:** 169–183.

Duguay, L. E., and D. L. Taylor. 1978. Primary production and calcification by the soritid foraminiferan *Archais angulatus* (Fichtel & Moll). *J. Protozool.* **25:** 356–361.

Eckert, R., and J. E. Chad. 1984. Inactivation of Ca channels. *Prog. Biophys. Molec. Biol.* **44:** 215–267.

Fisahn, J., T. McConnaughey, and W. J. Lucas. 1989. Oscillations in extracellular current, external pH, and membrane potential and conductance in the alkaline bands of *Nitella* and *Chara*. *J. Exp. Bot.* **40:** 1185–1193.

Garrels, R. M., A. Lerman, and F. T. Mackenzie. 1976. Controls of atmospheric CO_2 and O_2: past, present, and future. *Am. Sci.* **64:** 306–315.

Goreau, T. F. 1963. Calcium carbonate deposition by coralline algae and corals in relation to their roles as reef-builders. *Ann. N. Y. Acad. Sci.* **107:** 127–167.

Hayama, T., T. Shimmen, and M. Tazawa. 1979. Participation of Ca^{2+} in cessation of cytoplasmic streaming induced by membrane excitation in *Characeae* internodal cells. *Protoplasma* **99:** 305–321.

Jaffe, L. F., and R. Nuccitelli. 1974. An ultrasensitive vibrating probe for measuring extracellular currents. *J. Cell. Biol.* **63:** 614–628.

Kingsley, R. J., and N. Watabe. 1985. Ca-ATPase localization and inhibition in the gorgonian *Leptogorgia virgulata* (Lamarck) (Coelenterata: Gorgonacea). *J. Exp. Mar. Biol. Ecol.* **93:** 157–167.

Kishimoto, U., N. Kami-iki, Y. Takeuchi, and T. Ohdawa. 1984. A kinetic analysis of the electrogenic pump of *Chara corallina*: I. Inhibition of the pump by DCCD. *J. Membrane Biol.* **80:** 175–183.

Klaveness, D. 1976. *Emiliania huxleyi* (Lohman) Hay and Mohler. 3. Mineral deposition and the origin of the matrix during coccolith formation. *Protistologica* **12:** 217–224.

Kühtreiber, W. M., and L. F. Jaffe. 1990. Detection of extracellular calcium gradients with a calcium specific vibrating electrode. *J. Cell Biol.* **110:** 1565–1573.

Kuile, B. ter, J. Erez, and E. Padan. 1989. Mechanisms for the uptake of inorganic carbon by two species of symbiont-bearing foraminifera. *Mar. Biol.* **103:** 241–251.

Lucas, W. J. 1976. The influence of Ca^{2+} and K^+ on $H^{14}CO_3^-$ influx in internodal cells of *Chara corallina*. *J. Exp. Bot.* **27:** 32–42.

Lühring, H. and M. Tazawa. 1985. Effect of cytoplasmic Ca^{2+} on the membrane potential and membrane resistance of Chara plasmalemma. *Plant Cell Physiol.* **26:** 635–646.

MacRobbie, E. A. C., and J. Banfield. 1988. Calcium influx at the plasmalemma of *Chara corallina*. *Planta* **176:** 98–108.

McConnaughey, T. A. 1989a. Biomineralization mechanisms. Pp. 57–73 in *The Origin, Evolution, and Modern Aspects of Biomineralization in Animals and Plants*, R. E. Crick, ed. Plenum Press, New York.

McConnaughey, T. A. 1989b. ^{13}C and ^{18}O isotopic disequilibrium in biological carbonates. I. Patterns. *Geochim. Cosmochim. Acta* **53:** 151–162.

McConnaughey, T. A. 1989c. ^{13}C and ^{18}O isotopic disequilibrium in biological carbonates. II. *In vitro* simulation of kinetic isotope effects. *Geochim. Cosmochim. Acta* **53:** 163–171.

Miller, A. J., and D. Sanders. 1987. Depletion of cytosolic free calcium induced by photosynthesis. *Nature* **326:** 397–400.

Mimura, T., and Y. Kirino. 1984. Changes in cytoplasmic pH measured by ^{31}P-NMR in cells of *Nitellopsis obtusa*. *Plant Cell Physiol.* **25:** 813–820.

Niggli, V., E. Sigel, and E. Carafoli. 1982. The purified Ca^{2+} pump of human erythrocyte membranes catalyzes an electroneutral Ca^{2+}-H$^+$ exchange in reconstituted liposomal systems. *J. Biol. Chem.* **257:** 2350–2356.

Okazaki, M. 1977. Some enzymatic properties of Ca^{2+}-dependent adenosine triphosphatase from a calcareous marine alga, *Serraticardia maxima* and its distribution in marine algae. *Bot. Mar.* **20:** 347–354.

Okazaki, M., M. Fujii, Y. Usuda, and K. Furuya. 1984. Soluble Ca^{2+} activated ATPase and its possible role in calcification in the coccolithophorid *Cricosphaera roscoffensis var. Haptonemofera* (Haptophyta). *Bot. Mar.* **27:** 363–369.

Okazaki, M., and M. Tokita. 1988. Calcification of *Chara braunii* (Charophyta) caused by alkaline band formation coupled with photosynthesis. *Jpn. J. Phycol.* **36:** 193–201.

Okihara, K., and K. Kiyosawa. 1988. Ion composition of the *Chara* internode. *Plant Cell Physiol.* **29:** 21–25.

Paasche, E. 1964. A tracer study of the inorganic carbon uptake during coccolith formation and photosynthesis in the coccolithophorid *Coccolithus huxleyi*. *Physiol. Plant. Supp.* **III:** 5–82.

Pentecost, A. 1978. Calcification and photosynthesis in *corallina officinalis* L. using the ^{14}CO$_2$ method. *Br. Phycol. J.* **13:** 383–390.

Price, G. D., and M. R. Badger. 1985. Inhibition by proton buffers of photosynthetic utilization of bicarbonate in *Chara corallina*. *Aust. J. Plant Physiol.* **12:** 257–267.

Price, G. D., M. R. Badger, M. E. Bassett, and M. I. Whitecross. 1985. Involvement of plasmalemmasomes and carbonic anhydrase in photosynthetic utilization of bicarbonate in *Chara corallina*. *Aust. J. Plant Physiol.* **12:** 241–256.

Pringsheim, N. 1888. Uber die Entstehung der Kalkencrustationen an Susswasserpflanzen. *Jahrb. Wissensch. Bot.* **19:** 138–154.

Rasi-Caldogno, F., M. C. Pugliarello, and M. I. De Michelis. 1987. The Ca^{2+}-transport ATPase of plant plasma membrane catalyzes a nH$^+$/Ca^{2+} exchange. *Plant Physiol.* **83:** 994–1000.

Raven, J. A., F. A. Smith, and N. A. Walker. 1986. Biomineralization in the Charophyceae *sensu lato*. Pp. 125–139 in *Biomineralization in Lower Plants and Animals*, B. S. C. Leadbeater and R. Riding, eds. Clarendon Press, Oxford.

Sikes, C. S., R. D. Roer, and K. M. Wilbur. 1980. Photosynthesis and coccolith formation: inorganic carbon sources and net inorganic reaction of deposition. *Limnol. Oceanogr.* **25:** 248–261.

Smith, F. A. 1984a. Regulation of the cytoplasmic pH of *Chara corallina:* response to changes in external pH. *J. Exp. Bot.* **35:** 43–50.

Smith, F. A. 1984b. Regulation of the cytoplasmic pH of *Chara corallina* in the absence of external Ca^{2+}: its significance in relation to activity and control of the H$^+$ pump. *J. Exp. Bot.* **35:** 1525–1536.

Smith, F. A., and J. A. Raven. 1979. Intracellular pH and its regulation. *Ann. Rev. Plant Physiol.* **30:** 289–311.

Smith, F. A., and N. A. Walker. 1980. Photosynthesis by aquatic plants: effects of unstirred layers in relation to assimilation of CO$_2$ and HCO$_3^-$ and to carbon isotope discrimination. *New Phytol.* **86:** 245–259.

Spanswick, R. M., and A. G. Miller. 1977. Measurement of the cytoplasmic pH in *Nitella translucens*. *Plant Physiol.* **59:** 664–666.

Spanswick, R. M., and E. J. Williams. 1965. Ca fluxes and membrane potentials in *Nitella translucens*. *J. Exp. Bot.* **16:** 463–473.

Spear, D. G., J. K. Barr, and C. E. Barr. 1969. Localization of hydrogen ion and chloride ion fluxes in *Nitella*. *J. Gen. Physiol.* **54:** 397–414.

Stumm, W., and J. J. Morgan. 1970. *Aquatic Chemistry.* Wiley-Interscience, New York. 583 pp.

Tazawa, M., T. Shimmen, and T. Mimura. 1987. Membrane control in the characeae. *Ann. Rev. Plant Physiol.* **38:** 95–117.

Villalobo, A., and B. D. Roufogalis. 1986. Proton countertransport by the reconstituted erythrocyte Ca^{2+}-translocating ATPase: evidence using ionophoretic compounds. *J. Membr. Biol.* **93:** 249–258.

Walker, N. A., and F. A. Smith. 1977. Circulating electrical currents between acid and alkaline zones associated with HCO$_3^-$ assimilation in *Chara*. *J. Exp. Bot.* **28:** 1190–1206.

Walker, N. A., F. A. Smith, and I. R. Cathers. 1980. Bicarbonate assimilation by fresh-water charophytes and higher plants: I. Membrane transport of bicarbonate ions is not proven. *J. Membr. Biol.* **57:** 51–58.

Wiesenseel, M. H., and H. K. Ruppert. 1977. Phytochrome and calcium ions are involved in light-induced membrane depolarization in *Nitella*. *Planta* **137:** 225–229.